

## Computer-Assisted Bone Age Assessment: Graphical User Interface for Image Processing and Comparison

Ewa Pietka, PhD, DSc,<sup>1</sup> Arkadiusz Gertych, MS,<sup>1</sup> Sylwia Pospiech-Kurkowska, MS,<sup>1</sup>  
Fei Cao, PhD,<sup>2</sup> H.K. Huang, DSc,<sup>2</sup> and Vincente Gilzanz, MD, PhD<sup>2</sup>

The current study is part of a project resulting in a computer-assisted analysis of a hand radiograph yielding an assessment of skeletal maturity. The image analysis is based on features selected from six regions of interest. At various stages of skeletal development different image processing problems have to be addressed. At the early stage, feature extraction is based on Lee filtering followed by the random Gibbs fields and mathematical morphology. Once the fusion starts, wavelet decomposition methods are implemented. The user interface displays the closest neighbors to each image under consideration. Results show the sensitivity of different regions to both stages of development and certain feature sensitivity within each region. At the early stage of development, the distal features are more reliable indicators, whereas at the stage of epiphyseal fusion, a larger dynamic range of middle features makes them more sensitive. In the current study, a graphical user interface has been designed and implemented for testing the image processing routines and comparing the results of quantitative image analysis with the visual interpretation of extracted regions of interest. The user interface may also serve as a teaching tool. At the later stage of the project it will be used as a classification tool.

**KEY WORDS:** Skeletal maturity, bone age assessment, computer-aided diagnosis, feature extraction, image analysis, graphical user interface

**B**ONE AGE assessment is a radiological procedure performed for pediatric patients. A left-hand-wrist radiograph is acquired and compared with standard patterns. The diagnostic procedure is based on an overall comparison of the entire hand with an atlas pattern<sup>1</sup> or a detailed analysis of selected regions of interest.<sup>2</sup> Simplicity makes the first approach be used 76% of the time.<sup>3</sup> The dis-

advantage of this method is the subjective nature of the analysis performed by various observers with different levels of training. Studies have shown<sup>4</sup> interobserver differences ranging from 0.37 to 0.6 year, whereas the intraobserver differences range from 0.25 to 0.47 year. Atlas-matching methods have such high discrepancies because of a general comparison of the radiograph with the atlas pattern. By a more detailed comparison of individual bones, ambiguous results may be obtained.

Another technique of bone age assessment relies on a trained observer applying the Tanner and Whitehouse (TW2) method.<sup>2</sup> This method uses a detailed analysis of each individual bone (epiphysis – metaphysis complex of each tubular bone and carpal bones). Each complex is assigned to one of nine classes reflecting nine developmental stage<sup>2</sup>:

- stage A: lack of calcium deposit
- stage B: single deposit of calcium
- stage C: center is distinct in appearances
- stage D: maximum diameter is half or more the width of metaphysis
- stage E: border of the epiphysis is concave

---

<sup>1</sup>From the Division of Biomedical Electronics, Institute of Electronics, Silesian University of Technology, Gliwice, Poland.

<sup>2</sup>From the Department of Radiology, Children's Hospital Los Angeles, Los Angeles, CA, 90027, USA.

Correspondence to: Ewa Pietka, PhD, DSc, tel: +48 609 855 512; e-mail: pietka@polsl.gliwice.pl

Copyright © 2004 by SCAR (Society for Computer Applications in Radiology)

Online publication 13 July 2004

doi: 10.1007/s10278-004-1006-6

stage F: epiphysis is as wide as the metaphysis  
 stage G: epiphysis caps the metaphysis  
 stage H: fusion of epiphysis and metaphysis has begun  
 stage I: epiphyseal fusion completed

Assignment of each bony structure to a certain developmental stage is described in terms of scores. The sum of all scores reflects the overall stage of the skeletal development.

Several approaches have been made to the problem of computerized assistance in image diagnosis. A computer-assisted Tanner–Whitehouse (TW) method requires<sup>5</sup> an operator to position each epiphysis beneath a video camera, view the image on the computer screen, and match the image to the template of the developmental stages displayed on the screen. A Fourier transform yields coefficients that are compared with those generated by each stage of the TW standards and the closest match is sought. The computerized TW method has been evaluated in assessment of bone age<sup>6</sup> well as patients with Turner syndrome and constitutionally tall stature.<sup>7</sup>

Studies on certain hand regions have also been performed. Duryea et al<sup>8</sup> have developed an algorithm for the extraction of joint space and location of phalanx edges. Their approach<sup>9</sup> uses a cross-correlation as a measure of similarity between an analyzed region and a prototype. Another approach<sup>10</sup> performs the analysis of the middle region of the III phalanx. The method is based on a point distribution model derived by several points marked manually on the bones. This model is then compared with pattern models describing each developmental stage. A segmentation method based on the knowledge of anatomical structures has been suggested.<sup>11</sup>

This study is part of a project whose overall goal is to develop a computer-aided methodology able to assist the radiologist in assessment of skeletal maturity. The goal of this study is to develop a graphical user interface (GUI) able to view all stages of the image analysis. The GUI is used for testing purposes in order to analyze the reason for failures of certain image processing procedures and in clinical evaluation. The GUI is also applied in teaching and training programs.

## DATA

The analysis was performed on left-hand-wrist radiograms selected from a normal population and organized into four blocks: African–American male and female and European male and female. Based on preliminary results,<sup>12</sup> for prepubertal children (0 – 9 years old) 5 images for each age group were collected, whereas for children in puberty (10 – 18 years old) 10 images for each age group were collected. This yielded 135 images per block and a total of 540 images. These images were acquired at the USC Children's Hospital in Los Angeles.

A separate group of 1,000 clinical images (normal and pathological) was collected for evaluation. These images were acquired at the University of California, San Francisco. A Fuji FCR-9000 computed radiography (CR) system was used to acquire full-resolution CR images (2 kb × 2 kb × 10 bits) in a DICOM 3.0 standard. If analog technology was used, films were digitized with a Lumiscan 200 digitizer to 2 kb × 2 kb × 12 bits.

All images were stored in a Web-based environment database.<sup>13,14</sup> It included the hand images and their relevant patient data. The system architecture was separated into two parts: One served as a data collection part and the other was a hand atlas server. Reference and clinical hand image were stored on an Oracle Image Database Server.

## IMAGE PREPROCESSING PROCEDURES

Graphical user interface views three stages of the image analysis. The first stage performs the image standardization including the background suppression and removal of markers, labels, and noisy objects. Then, features sensitive to a certain stage of development are extracted. Finally, images from the reference database, whose features fulfill the closest match, are selected and corresponding regions of interest are displayed.

### Background Removal

Background extraction<sup>15</sup> is based on a joint analysis of a set of histograms. The tallest peak of a global histogram reflecting the soft and

bony structure is mapped onto four local histograms of four image quarters. Locations of the tallest local peaks correspond to the average intensity of the background level. Because of background nonuniformity, these levels have to be found independently. They serve as a basis for the overall background estimation found by the means of a bilinear interpolation.

After the background removal a global histogram features a narrow peak reflecting the hand area. A triangle algorithm points to the threshold value which permits the hand to be extracted. Morphological operators remove isolated points.

### Extraction of the Epiphyseal Region of Interest

After the hand area has been extracted, the epiphyseal regions of interest (EROI) of the II, III, and IV phalanges are located (Fig. 1). Along phalangeal axes first-order derivative vectors are searched for three local maxima reflecting the gaps between epiphyses and metaphyses. An insensitivity sector which covers the entire area surrounding the gap prevents two neighbor maxima from being selected within the same epiphyseal region.<sup>15</sup>

Once the gaps are located, the EROI edges are defined. The width is estimated by the distance between the phalangeal edges and the height is set on the basis of the neighbor gap location.

### GRAPHICAL USER INTERFACE

Because of the changes in bony structures, skeletal development is divided into two stages. In the first stage the epiphyses change in size filling up the gap between epiphyses and metaphyses. Once the mature size is reached, both bones start to fuse. The process starts from the middle and expands toward the edges.

Features describing the developmental stage differ from one stage to the other. As long as the epiphyseal size is changing, the diameters can be used as sensitive parameters. Once the size does not differ, features measuring the stage of fusion have to be extracted. Since the nature of the features differs significantly, the extraction techniques vary as well. In order to view the

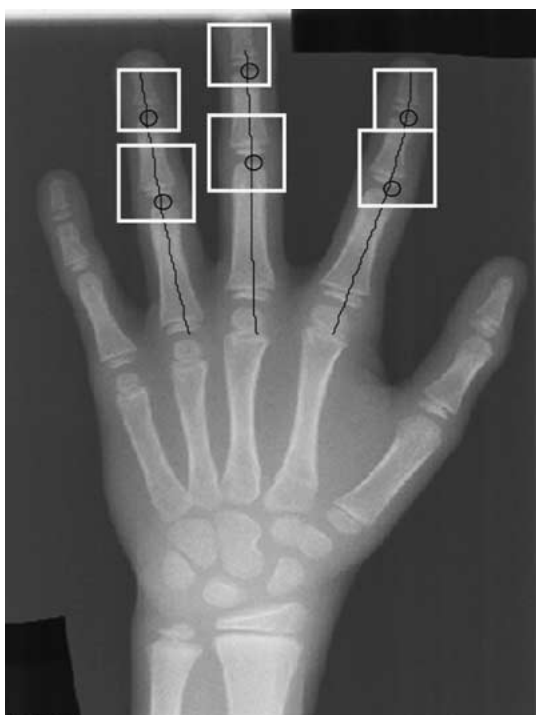


Fig 1. Epiphyseal regions of interest of the II, III, and IV phalanges.

image function performed in both developmental stages, the GUI is designed independently for both phases.

### Early Stage of Skeletal Development

The early stage of skeletal maturity requires a detailed analysis of the size and shape of epiphyses and metaphyses. The flowchart of the EROI processing performed by the GUI is shown in (Figure 2). The main menu of the GUI is divided into two sections (Fig. 3). First, the filtration permits testing various filters and viewing the processed region next to each other for comparison. The second section turns on the segmentation and features extraction stages. After the region is viewed by using the **Load Image** button, various filtering techniques may be tested.

#### *Filtration*

The median filter replaces each pixel by the median of its neighborhoods. All eight neighborhoods may be chosen or a star-shaped area may be tested. This is defined as:

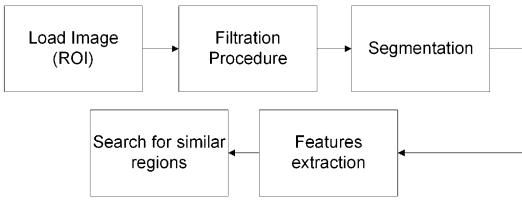


Fig 2. Flowchart of EMROI processing.

$$y(i,j) = \text{median}|x(i,j), x(i,j+1), x(i,j-1), x(i-1,j), x(i+1,j)|, \quad (1)$$

where  $i, j$  are pixel coordinates,  $x$  is the input image, and  $y$  is the output image. The function suppresses the impulse noise (“salt and pepper”) and smoothes the nonuniformity within the soft tissue and bony structure. At this step, a median filter or star-shaped median filter can be tested followed by Lee filtration.<sup>16</sup> The mask size of each filter is set to  $3 \times 3$ .

Lee’s filter is given by

$$p(i,j) = m_f(i,j) + \frac{\sigma_f^2(i,j)}{\sigma_f^2(i,j) + \sigma_v^2} [g(i,j) - m_f(i,j)], \quad (2)$$

where  $p(i,j)$  is a processed image (output image),  $g(i,j)$  is a corrupted image (input image),  $m_f(i,j)$  and  $\sigma_f(i,j)$  are local mean and standard deviation of original image,  $\sigma_v^2$  is a noise variance, and  $i,j$  are pixel coordinates.

The filtration procedure requires the noise variance  $\sigma_v^2$  to be known. If the noise variance is not given, the algorithm uses the average of all local estimated variances. Other parameters such as  $m_f(i,j)$  and  $\sigma_f(i,j)$  are estimated from the input image and delimited by a  $3 \times 3$  mask. A larger mask smoothes the edges. This is particularly undesirable in images of optimally chosen exposure parameters yielding sharp variation edges.

### Segmentation and Features Extraction

Both filtered and unfiltered (original) regions can be subjected to further analysis. Its goal is to separate the bony structure from soft tissue.

The segmentation procedure consists of two steps: (1) a preliminary clustering step applying a  $c$ -means algorithm and (2) segmentation with Gibbs random fields and estimation of intensity function.

A  $c$ -means clustering algorithm<sup>17</sup> uses a similarity measure based on the Euclidean distance between samples and cluster prototypes. Each  $k$ th sample (pixel) has three components: image coordinates and gray level. The samples are grouped into a predefined number of classes. A criterion of partitioning is based on the minimization of the relative difference between prototypes in two iterations.

The goal of the second step of the segmentation procedure is to assign the image pixels to a certain class on the basis of their intensity and relative location. In our model, a pixel  $y$  of the image is at a location  $s$  and its intensity (gray level) is  $y_s$ . A segmentation (subdivision) of the image into classes will be denoted by  $x$ , where  $x_s = i$  means that a pixel belongs to the class  $i$ . In our approach the number of classes is set to 2. Each class can be described by a slowly varying intensity function plus white Gaussian noise having a  $\sigma_n^2$  noise variance. In order to make use of the spatial information, a Gibbs random field describing local distribution of gray levels is used. Given the intensity function, a probability density function having two components can be defined. One constrains the region intensity to be close to the data, the other imposes spatial continuity. The algorithm maximizes the probability density function and estimates the intensity functions alternately. As the algorithm progresses, the intensities are updated by averaging gray level values of pixels belonging to the considered classes over the sliding window whose size progressively decreases. Thus, the algorithm starts with global estimates and slowly adapts to the local characteristics of each class<sup>18,19</sup>(Fig. 4a). In our model only one-point and two-point cliques are applied (Fig. 4b). The noise parameter is calculated by a distinct procedure however, the user is able to set its value manually (Fig. 3).

The  $c$ -means clustering algorithm initially estimates  $x$ . Beginning with segmentation (Fig. 4a), the algorithm estimates intensity functions  $\mu_s^{(i)}$  and  $x$  interchangeably. Each iteration consists of one update of  $x$  and one up-

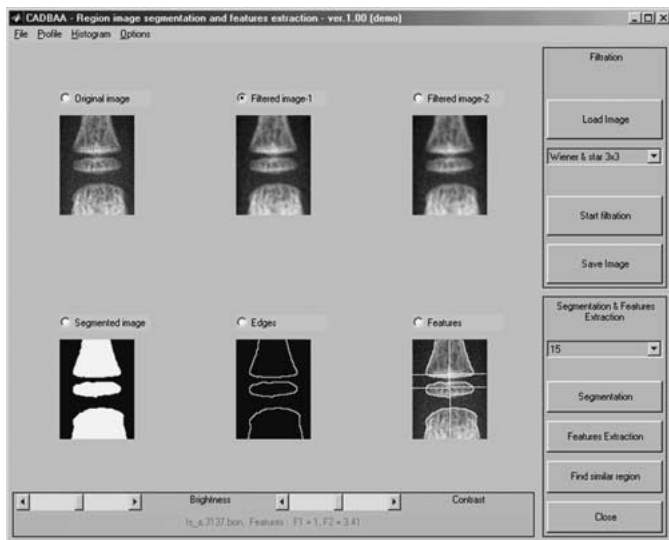


Fig 3. Program main window.

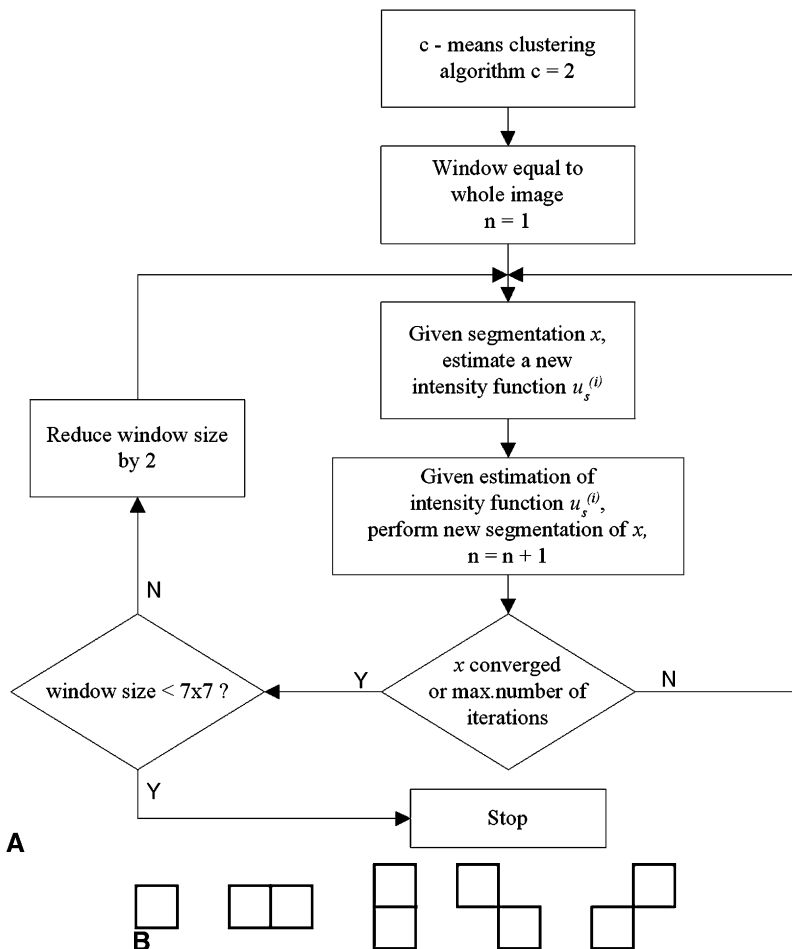


Fig 4. Segmentation procedure: (a) the flowchart, (b) one-point and two-point cliques.

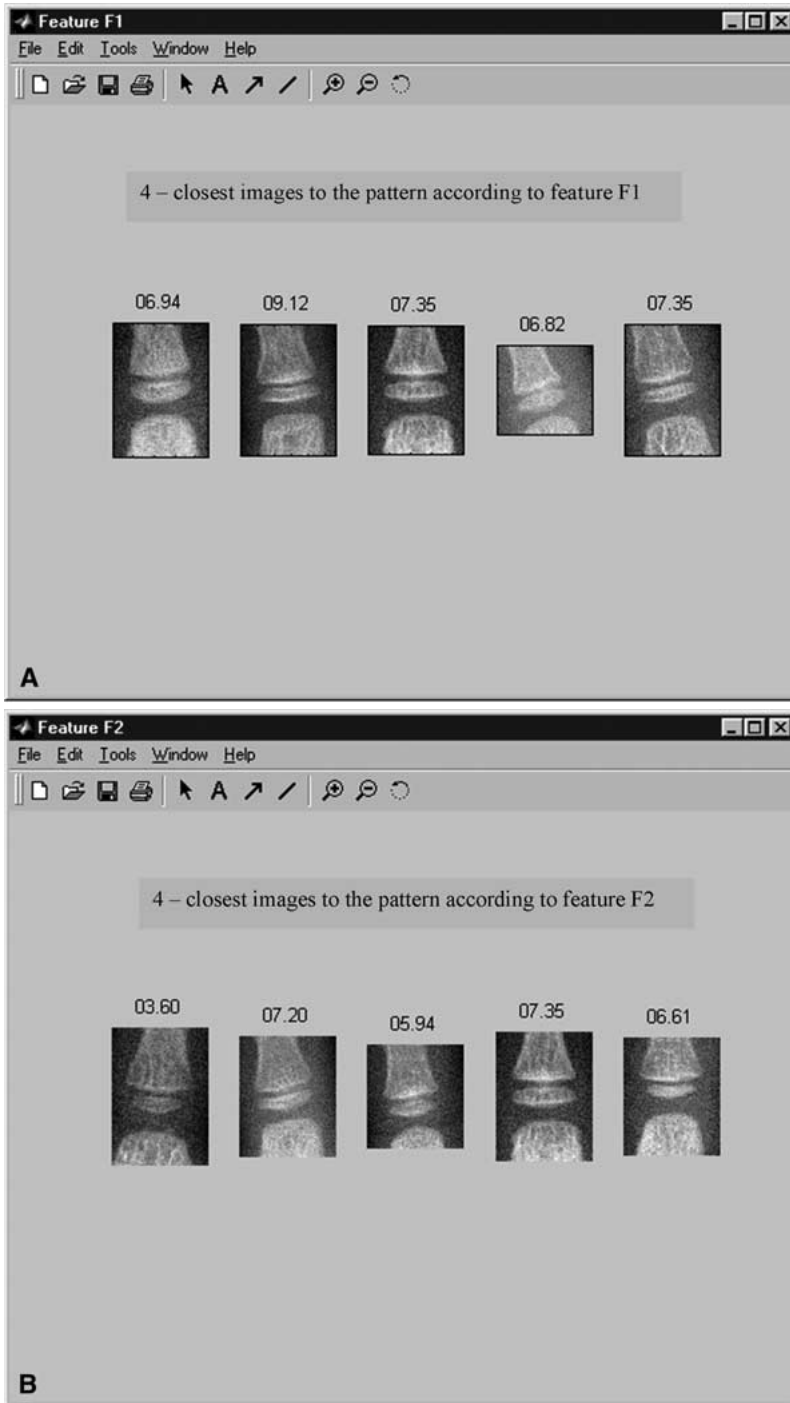


Fig 5. The most similar regions according to features: (a) F1, (b) F2.

date of intensity functions  $\mu_s^{(i)}$ . Based on the estimation of intensity functions  $\mu_s^{(i)}$  and maximization of the conditional density at each

point  $x_s$ , the current pixel  $x$  assignment to one of the classes is updated. Until the procedure converges, the window size  $W$  for calculating



Fig 6. Image info window.

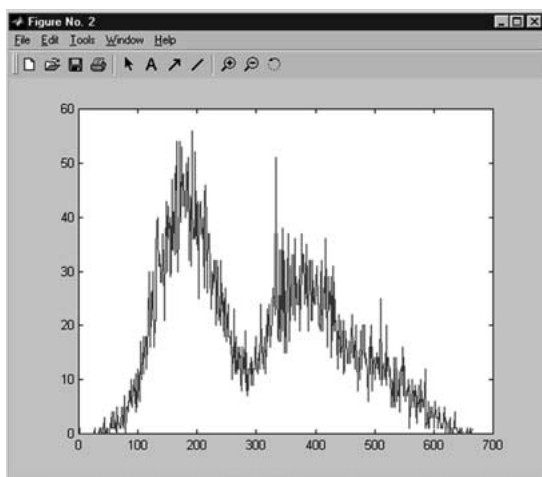


Fig 7. Sample histogram of original image.

### *Bone Edge and Feature Extraction*

The segmentation procedure yields a binary image (Fig. 3) in which the bony structure appears as white objects, whereas other areas (background and soft tissue) turn to black. This binary image is subjected to a further image analysis. In order to draw edges between white and black objects, a perimeter morphological operation is implemented. A white pixel belongs to the perimeter if there is at least one black pixel in its eight-closest neighborhoods. Next, for removing one-pixel white objects, the cleaning morphological operation is performed. A white pixel is removed if it is surrounded by eight black pixels.

Two morphological operations, a perimeter PM and a cleaning pixel operate CP, are defined as:

$$PM(i,j) = X \cap (\overline{X_0} \cup \overline{X_1} \cup \dots \cup \overline{X_7})$$

$$CP(i,j) = X \cap (X_0 \cup X_1 \cup \dots \cup X_7)$$

The main goal of morphological operations is to prepare the binary image for the main axis extraction. In this step, only the first and the last white pixel in each row of the binary image are considered as the bone-soft tissue edge. The important improvement at this step in comparison to previous work<sup>20</sup> is that the object contours are continuous.

Once the *Features extraction* option from the menu (Fig. 3) is selected, three steps are laun-

the intensity estimations is fixed. Then the whole procedure is repeated with a new window size. Initially, the window size is equal to the image size and thus the intensity functions of each region are uniform. In the course of iterations, the window size decreases by a factor of 2 until the minimum window size ( $7 \times 7$  [pixel]) is reached. The estimation of  $x$  converges if the number of pixels that changes during a cycle is less than a threshold, typically  $M/10$  (where  $M$  is the smallest image dimension).

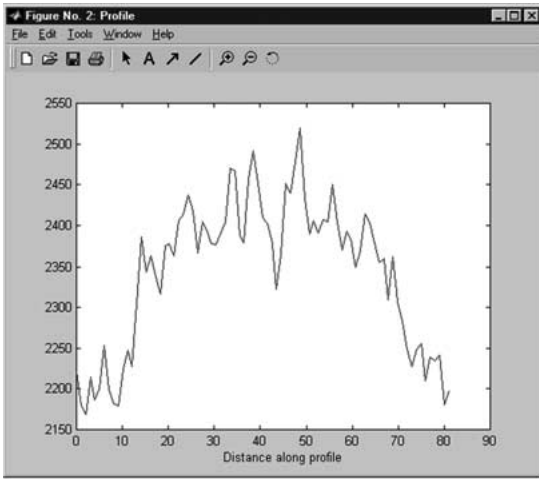


Fig 8. Distance along profile.

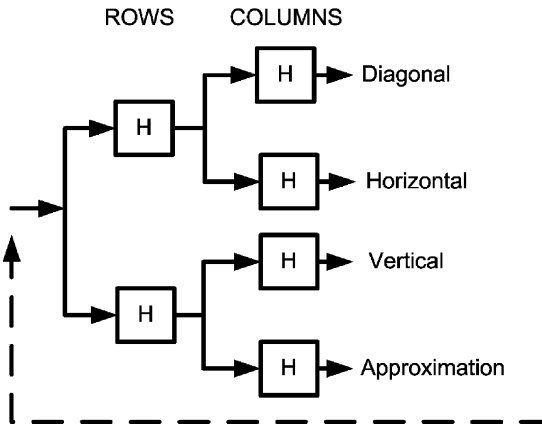


Fig 9. Wavelet decomposition algorithm scheme (first iteration).

ched. First, the main axis of each phalanx (metaphyses) is found. Then, the image is scanned perpendicular to the main axis. At this point the transverse dimensions of the metaphysis and epiphysis are located. If the segmented image contains three distinct objects (area of metaphysis, epiphysis, and diaphysis), immediately the extraction of epiphyses is proven. Finally, the epiphyseal vertical diameter is found along the main axis. Based on these findings, two features are extracted: the ratio of both transverse dimensions and the ratio of both epiphyseal dimensions marked F1 and F2, respectively.

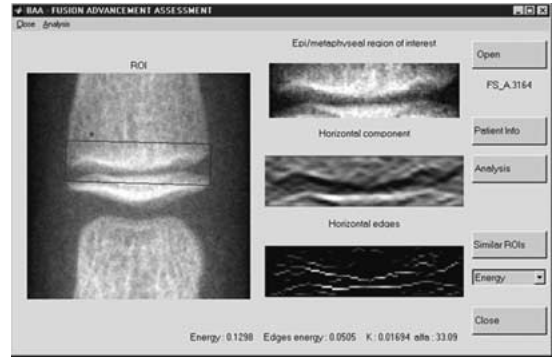


Fig 10. Epiphyseal fusion assessment. Left: EMROI with marked epiphyseal region to be analyzed. Right top: epiphyseal region to be analyzed after the alignment; middle: horizontal component of the wavelet decomposition, bottom: horizontal edges.

### Search for Similar Region

All images of the control group have been subjected to image analysis and both features (F1 and F2) have been derived. They serve as a standard data for image comparison. Once the *Find similar region* option is selected, the four most similar images from the database are displayed. The similarity is measured as the Euclidean distance between features (Fig. 5).

Additional options implemented in the GUI include (Fig. 6) patient information (sex, date of birth, age, height, weight, Tanner index) displayed by selecting the **Image Info** button from the main menu. In order to enhance the image, adjustment of brightness/contrast and zoom can be applied. More advanced options such as profiles and histograms are implemented. This may be especially helpful in a case of a manual parameter measurement. In each case a new window appears and a histogram (Fig. 7) or gray level values along the chosen profile (Fig. 8) are drawn. At any time the user may save the image for further analysis by clicking the **Save image** button or selecting *Save* from the *File* menu (Fig. 3).

## Later Stage of Skeletal Development

### Methodology of Feature Development

In our study the late stage of skeletal development is the stage in which the epiphyseal fusion progresses. It starts approximately at the

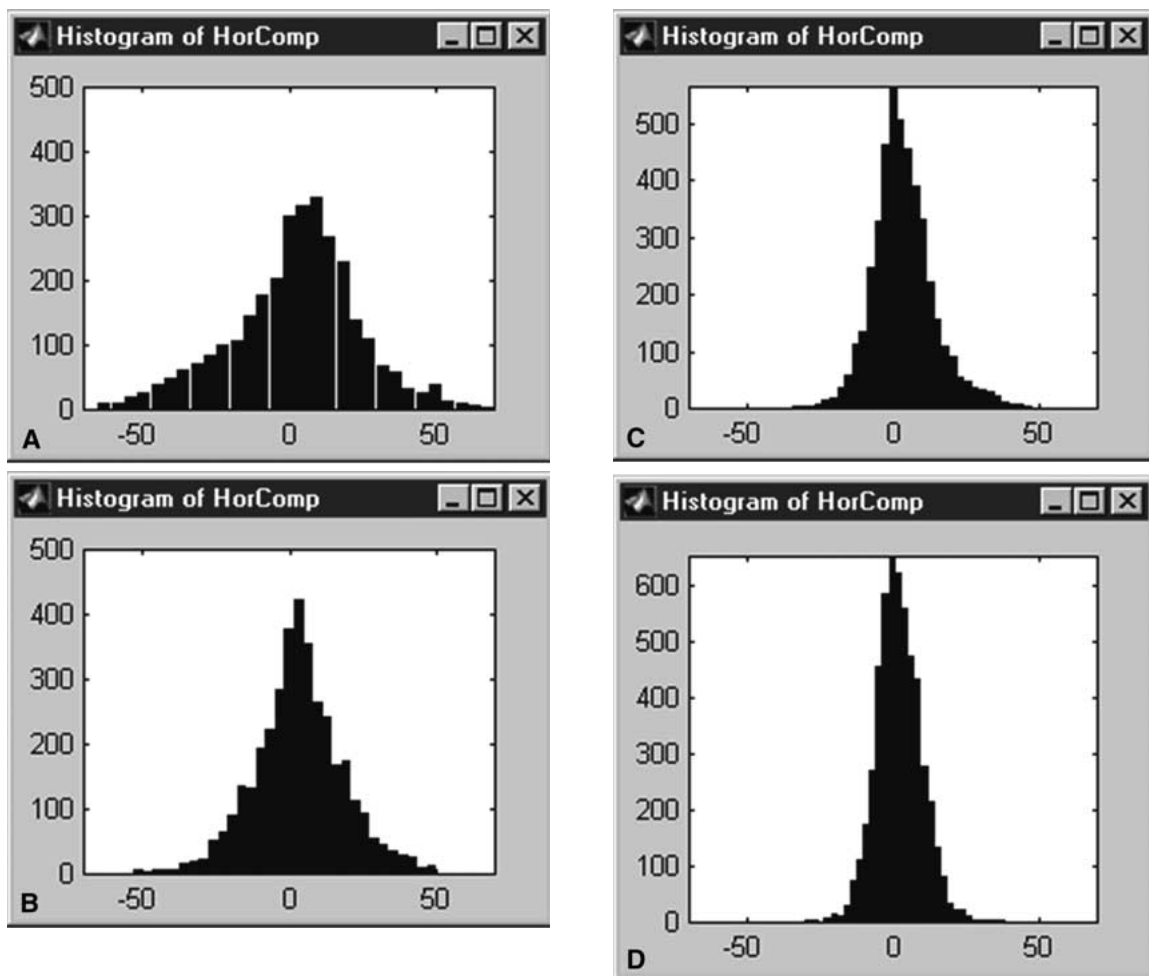


Fig 11. Results of the database match according to (a) energy of horizontal component; (b) energy of horizontal edges; (c) histogram parameter  $K$ ; (d) histogram parameter  $\alpha$ .

age of 10 in girls and 12 in boys and continues until the epiphysis and metaphysis become one adult bone. Features measuring the size of bones are no longer pertinent at this developmental stage. The assessment of the fusion stage is performed by means of the wavelet decomposition. In our study, the most important property of the 2-dimensional separable wavelet transform is its ability to separate vertical, diagonal, and horizontal structures of an image. The separation is achieved by convolving the image with low- and high-pass wavelet filters along the rows and columns.<sup>21</sup> The decomposition yields an approximation component and three detailed components: vertical, horizontal, diagonal (Fig. 9).

It can be noticed that the advancement of epiphyseal fusion suppresses horizontal edges of bones. At this stage features reflecting the presence of edges have to be defined and extracted. The analysis is performed on the horizontal component of the wavelet decomposition. Unlike in the standard decomposition scheme, in the current study the image is not subsampled after each level.

An analysis of the epiphyseal – metaphyseal ROI (EMROI) begins with an alignment approval. If the angle of the phalangeal axis and the vertical direction exceeds  $5^\circ$ , a rotation procedure is applied. Quantitative analysis requires a precise definition of the region: It is limited to the upper part of the epiphysis and metaphysis

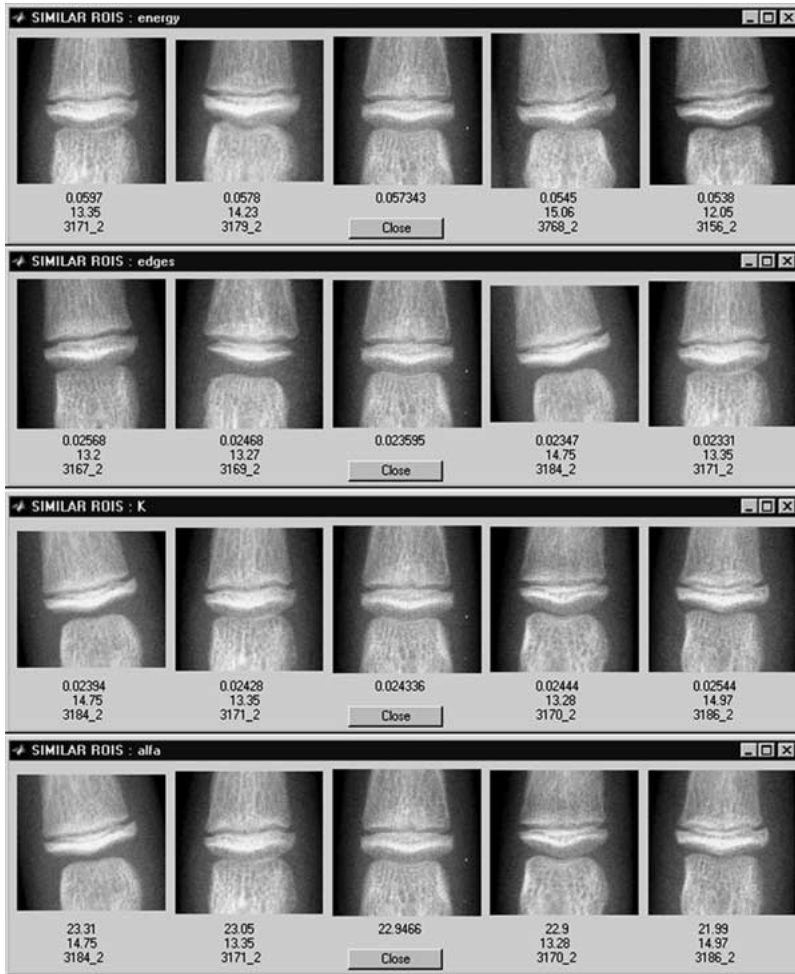


Fig 12. Histogram of horizontal component at different stages of fusion: from epiphysis and metaphysis not fused to a complete fusion.

(Fig. 10). The already marked transverse dimensions delimit the region. Next, the decomposition algorithm is applied. It is based on the biorthogonal, Haar, and Mallat wavelet filters.<sup>22</sup> Coefficients of original filters  $L_1$  and  $H_1$  are shown in Table 1. Because of the size of the regions subjected to the wavelet transform (an average of 30–40 rows), using short high-pass filters is an important advantage.

Features applied to the estimation of the stage of fusion are calculated for the horizontal detail component at the second level of decomposition.<sup>23</sup> In order to extract the horizontal edges, local maxima of the horizontal component along columns are found. Then, a thresholding procedure is applied. The thresh-

old value is estimated on the basis of the standard deviation of the combination of the horizontal and vertical components. This procedure enhances the main vertical edges.

Two coefficients sensitive to the developmental process have been chosen.<sup>24</sup> They are derived from the energy of horizontal details:

$$C1 = E(H)/E(\text{ROI}) \quad (3)$$

and the energy of horizontal edges, defined as

$$C2 = E(Y)/E(\text{ROI}) \quad (4)$$

Parameters  $K$  and  $\alpha$  of a histogram model also reflect the advancement of the epiphyseal fusion:

**Table 1. Wavelet decomposition filters used in BAA-Fusion Advancement Unit.**

Filter <sup>a</sup>	$L_1$	$H_1$
biorl.3	-0.08838834764832	0
	0.08838834764832	0
	0.70710678118655	-0.70710678118655
	0.70710678118655	0.70710678118655
	0.08838834764832	0
Haar	-0.08838834764832	0
	0.70710678118655	-0.70710678118655
Mallat	0.70710678118655	0.70710678118655
	0.12500	0
	0.37500	-2.0
	0.37500	2.0
biorl.5	012500	0
	0.01657281518406	0
	-0.01657281518406	0
	-0.12153397801644	0
	0.12153397801644	0
	0.70710678118655	-0.70710678118655
	0.70710678118655	0.70710678118655
	0.12153397801644	0
	-0.12153397801644	0
	-0.01657281518406	0
bior2.2	0.01657281518406	0
	0	0
	-0.17677669529664	0.35355339059327
	0.35355339059327	-0.70710678118655
bior2.4	1.06066017177982	0.35355339059327
	0.35355339059327	0
	-0.17677669529664	0
	0	0
	0.03314563036812	0
	-0.06629126073624	0
	-0.17677669529664	0.35355339059327
	0.41984465132951	-0.70710678118655
	0.99436891104358	0.35355339059327
	0.41984465132951	0
-0.17677669529664	0	
db2	-0.06629126073624	0
	0.03314563036812	0
	-0.12940952255092	-0.48296291314469
	0.22414386804186	0.83651630373747
	0.83651630373747	-0.22414386804186
	0.48296291314469	-0.12940952255092

<sup>a</sup> Filters: Biorl.3, Haar and Mallat are implemented for fusion assessment, the others are implemented for comparison.

$$h(u) = Ke^{-(|u|/\alpha)^\beta} \quad (5)$$

where  $H$  is the horizontal component at the second level of decomposition,  $Y$  is the horizontal edge at the second level of decomposition, ROI is the epiphyseal region of interest,  $E$  is the energy defined as

$$E(X) = \sum_{ij} x_{ij}^2$$

$h(u)$  is the histogram,  $K$  is a normalization constant,  $\alpha$  is the width of the histogram peak, and  $\beta$  is the decreasing rate (not related to the fusion advancement).

$K$ ,  $\alpha$ , and  $\beta$  are calculated as:

$$K = \frac{\beta}{2\alpha\Gamma(1/\beta)}, \quad \alpha = m_1 \frac{\Gamma(1/\beta)}{\Gamma(2/\beta)}, \quad \beta = F^{-1}\left(\frac{m_1^2}{m_2}\right)$$

$$\Gamma(x) = \int_0^\infty e^{-t} t^{x-1} dt, \quad F(x) = \frac{\Gamma^2(2/x)}{\Gamma(3/x)\Gamma(1/x)} \quad (6)$$

$$m_1 = \int |u|h(u)du, \quad m_2 = \int |u|^2 h(u)du$$

In order to reduce the influence of radiological exposure, two coefficients are defined as ratios. The first, Eq. 3, finds the energy of the horizontal component with respect to the energy of the original ROI. The second Eq. 4, divides the energy of edges by the energy of the original ROI 2 (Eq. 4). Thus, the coefficients can be interpreted as a fraction of the energy of the entire horizontal component or horizontal edges of the original region. The histogram model (Eqs. 5 and 6) describes the texture.<sup>21,25</sup> Three parameters have been considered for the assessment of the fusion stage, yet one of them ( $\beta$ ) is not sensitive to fusion advancement. Histograms of the horizontal component at different stages of fusion are shown in Figure 11. It is noted that the peak gets taller and narrower when the gap disappears.

### Fusion Assessment Unit

The fusion assessment window is shown in Figure 10. As described above, the **Open** button allows the user to select and load a ROI. The **Analysis** button invokes the wavelet decomposition and feature extraction. This results in the following images being displayed: aligned region to be analyzed, horizontal component, and horizontal edges. Values of features are listed below. Three types of wavelets filters (bioorthogonal, Haar, Mallat) at different decomposition levels can be tested by changing (in the

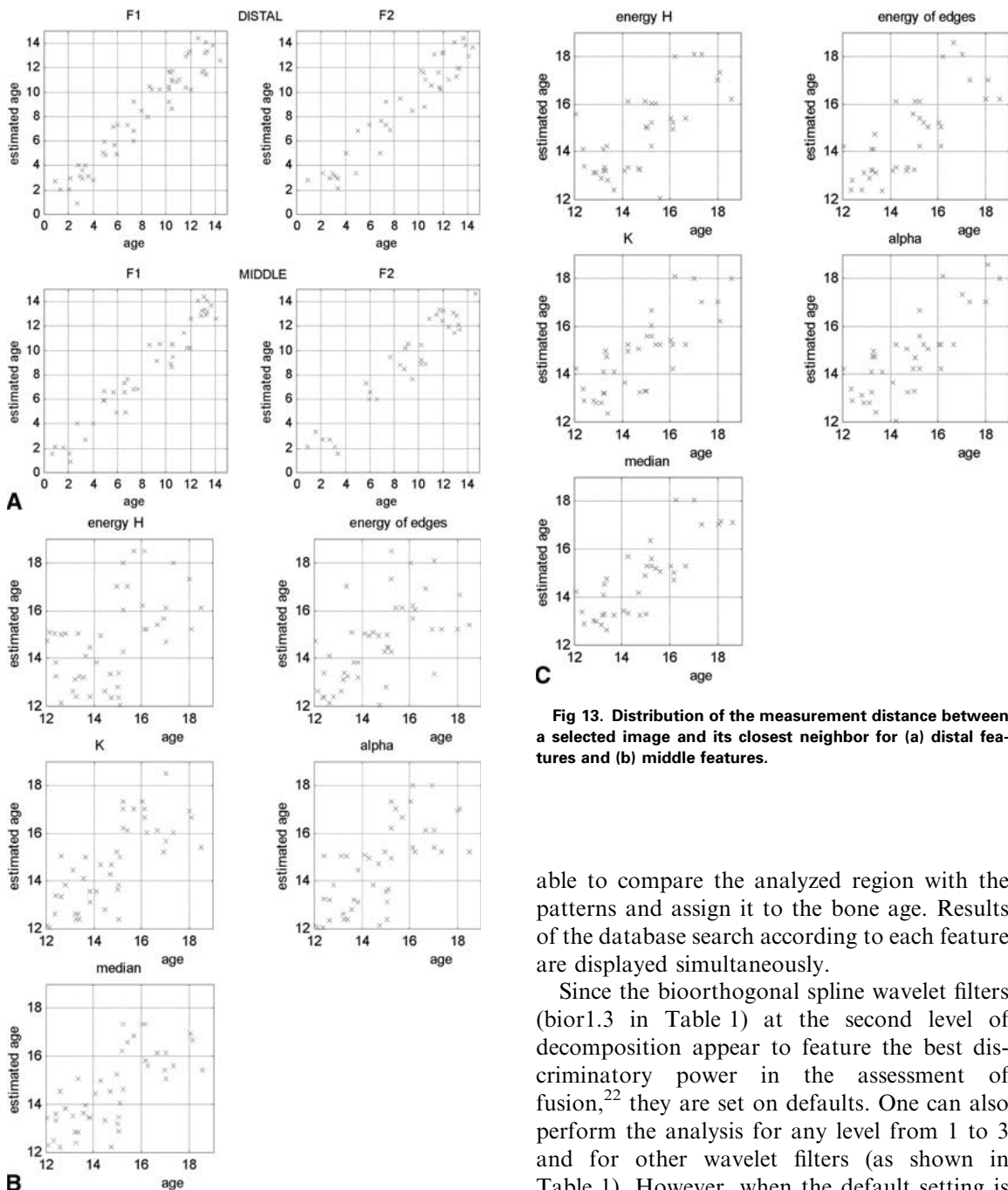


**Fig 13. Distribution of the measurement distance between a selected image and its closest neighbor for (a) distal features and (b) middle features.**

able to compare the analyzed region with the patterns and assign it to the bone age. Results of the database search according to each feature are displayed simultaneously.

Since the bioorthogonal spline wavelet filters (bior1.3 in Table 1) at the second level of decomposition appear to feature the best discriminatory power in the assessment of fusion,<sup>22</sup> they are set on defaults. One can also perform the analysis for any level from 1 to 3 and for other wavelet filters (as shown in Table 1). However, when the default setting is changed a **similar ROIs** search becomes inactive as comparison of parameters calculated for different levels or filters makes no sense. The **Patient Info** button displays the information from the ROI file header. After displaying a new ROI, **Patient Info** and **Analysis** buttons are active and **Feature Selection** and **Similar ROIs** buttons are inactive.

menu) the default settings. After the analysis is completed the user can select one of the features and search for similar regions in the database. On default four regions are displayed, two on both sides. The feature value, age of a child, and ID of the displayed image are listed below each of the reference regions (Fig. 12). The user is

## RESULTS AND CONCLUSION

The GUI has been developed as a tool for the comparison of quantitative image analysis with the appearance of changes in the image. The analysis has been performed for one ethnic group and one gender. Two steps of the evaluation have been performed. First, a quantitative analysis of features has shown the accuracy of the assessment of the image similarity. Then, the four closest neighbor images have been selected and displayed.

In the current study images from the normally developed population have been considered and the similarity of features has served as a basis for the image comparison. Therefore, the chronological age corresponds to the skeletal age. For each image the features have been found. Then, the image of the closest feature has been selected from the database. By selecting the closest match, plots (Fig. 13) show the deviation of the skeletal age within the standard database. The distribution varies for different features. A percentage of images with 3 standard deviations serves as an indicator in the analysis of feature sensitivity. For the younger population, the ratio of horizontal diameters (F1) matches images with a better similarity (Fig. 13a) than the ratio of epiphyseal diameters in vertical and horizontal diameters (F2). The distal regions show a higher discriminatory power than the middle regions. For the older population (Fig. 13b, c), features extracted from the middle regions are better indicators for image matching than the corresponding features of the distal regions.

As far as the visual comparison is concerned, there is no significant difference between the analyzed image and two closest neighbors, yet there is a visible difference if four closest neighbors are displayed.

Results have shown various sensitivity of features extracted from both regions. The distal ROIs yield better results in the earlier stage of development. A closer match is obtained and the mean distance between an image and its closest neighbor is smaller for distal features. It differs at the latter stage of development. Features extracted from the middle regions show a better sensitivity in differentiating various stages of development. These conclusions are in

accordance with the medical statement; "The more distal, the better"<sup>26</sup>. The distal areas feature a higher sensitivity to the developmental changes and reach the mature size and shape earlier than middle regions. Thus, after a certain stage of development, the middle regions show a larger dynamic range than the more mature distal areas.

The user interface is implemented for testing and teaching purposes well. It permits certain stages of the image analysis to be visualized. The influence of processing parameters can be examined and their adjustment improves the performance of the overall analysis.

Finally, the GUI will be applied at the classification stage when clinical images will be subjected to bone age assessment. In the final clinical implementation of the entire computer-aided system, it will be used as an assistance procedure in performing radiological diagnosis. Access to the closest image and its display will improve the objectivity and speed up the radiological procedure.

## ACKNOWLEDGMENT

This work was supported in part by KBN 7711C 03320 and in part by NIH Grant No.ROI-LM06270.

## REFERENCES

1. Greulich, WW, Pyle, SI: Radiographic Atlas of Skeletal Development of Hand Wrist 2nd ed. Stanford, CA: Stanford University Press, 1971
2. Tanner, JM, Whitehouse, RH: Assessment of Skeletal Maturity and Prediction of Adult Height (TW2 Method). London: Academic Press, 1975
3. Miler, GR, Levick, RK, Kay, R: Assessment of bone age: A comparison of the Greulich and Pyle and the Tanner and Whitehouse methods. *Clin Radiol* 37:119-121, 1986
4. Roch, AF, Rohmann, CG, Davila, GH: Effect of training on replicability of assessment of skeletal maturity (Greulich-Pyle). *AJR Am J Roentgenol*, 108:511-515, 1970
5. Tanner, JM, Gibbons, RD: Automatic bone age measurement using computerized image analysis. *J Pediatr Endocrinol* 7:141-145, 1994
6. Albanese, A, Hall, C, Stanhope, R: The use of a computerized method of bone age assessment in clinical practice. *Horm Res* 3:2-7, 1995
7. van Teunenbroek, A, de Waal, W, Rock, A, et al: Computer-aided skeletal age scores in healthy children, girls with Turner syndrome, and in children with constitutionally tall stature. *Pediatr Res* 39:360-367, 1996

8. Duryea, J, Jiang, Y, Countryman, P, Genant, HK: Automated algorithm for the identification of joint space and phalanx margin location on digital hand radiographs. *Med, Phys* 26:453-461, 1999
9. Dickhaus H, Habich R, Wastl S, et al: A PC-based system for bone age assessment. In proceedings of the EMBC '99, Vienna, Medical Imaging IV, 1999, pp 1008–1009
10. Al-Taani AT, Ricketts IW, Cairns AY: Classification of Hand Bones for Bone Age Assessment. In Proceedings of the 3rd IEEE International Conference on Electronics, Circuits and Systems (ICECS '96), October 1996, Greece, Vol 2, pp 1088–1091 (ISBN 0-7803-3650-X (softbound) and ISBN 0-7803-3651-8 (microfiche)
11. Efford, ND: Knowledge-based segmentation and feature analysis of hand and wrist radiographs. *proc SPIE* 1905:596-608, 1993
12. Pietka, E, Huang, HK: Image processing techniques in bone age assessment In: Leondes, CT ed. *Image Processing Techniques and Applications* Gordon & Breach Publishers, Inc., London, 1997, pp 221-272
13. Cao, F, Huang, HK, Pietka, E, et al: Design and implementation of a digital hand atlas for Web-based bone age assessment. *Radiology* 217(P):685, 2000
14. Cao, F, Huang, HK, Pietka, E, et al: A digital hand atlas for Web-based bone age assessment: System design and implementation. *SPIE Med Imaging* 3976:297-307, 2000
15. Pietka, E, Poépiech, S, Gertych, A, et al: Computerized approach to the extraction of epiphyseal regions in hand radiographs. *J Digital Imaging* 14(14):165-172, 2001
16. Lim, JS: *Two Dimensional Signal & Image processing* Prentice-Hall, Englewood Cliffs, UJ, 1990, pp 536-540  
Image Restoration
17. Banks, S: *Signal Processing, Image Processing and Pattern Recognition* Englewood Cliffs, NJ: Prentice-Hall, 1990
18. Pappas, T: An adaptive segmentation algorithm for image segmentation. *IEEE Trans, Signal Proc.* 40(4):901-914, 1992
19. Saber, E, Murat Tekalp, A, Bozdagi, G: Fusion of color and edge information for improved segmentation and edge linking. *Image Vision Comput* 15:769-780, 1997
20. Pietka, E, Gertych, A, Poépiech, S, et al: Computer assisted bone age assessment: Image preprocessing and ROI extraction, *IEEE Trans. Med. Imaging* 20(8):715-729, 2001
21. Mallat, SG: A theory for multiresolution signal decomposition: the wavelet representation. *IEEE Trans Patt Anal Mach. Int* 11(7):674-693, 1989
22. Mallat, S, Zhong, S: Characterization of signals from multiscale edges. *IEEE Trans-Patt, Anal, Mach, Int.* 14(7):710-732, 1992
23. Poépiech S: Assessment of epiphyseal fusion by means of wavelet transform. Proceedings of the International Workshop on Control and Information Technology, IWCIT'99 Ostrava, 1999, pp 248–254
24. Poépiech S, Gertych A, Pietka E, et al: Wavelet decomposition based features in description of epiphyseal fusion. In: Analysis of biomedical signals and images. Proceedings of BIOSIGNAL, Brno, 2000, pp 246–248 Vutium Press
25. Wouwer, G Van de , Scheunders, P, Dyck, D Van : Statistical texture characterization from discrete wavelet representations. *IEEE Trans Med, Imaging* 8(4):592-598, 1999
26. Kirks, DR: *Practical Pediatric Imaging. Diagnostic Radiology of Infants and Children* Little, Brown, Boston/Toronto, 1984, Chap. 6 pp 198-201